RSC Advances

PAPER

View Article Online
View Journal | View Issue

Open Access Article. Published on 22 December 2021. Downloaded on 11/8/2025 3:00:16 AM.
This article is licensed under a Creative Commons Attribution-NonCommercial 3.0 Unported Licence.

Check for updates

Cite this: *RSC Adv.*, 2022, **12**, 429

Debunking the essential effect of temperature and voltage on the current curve and the nanotube morphology

Tianle Gong,†[a] Jieda Chen,†[a] Pengjin Fang,[b] Lin Liu,*[b] Chengyuan Li,[a] Aijun Han[a] and Ye Song*[a]

The formation mechanism of anodic TiO_2 nanotubes remains to be unclear till now. Many researchers study the influence of temperatures above 0 °C instead of below 0 °C. Few papers before have explained the relationship between the current–time curve and the morphology of the nanotubes. In this study, the innovative 'oxygen bubble model' and the ionic current and electronic current theories were introduced to explain the growth of nanotubes below 0 °C. The length of anodic TiO_2 nanotubes at 15 °C, 0 °C, −10 °C were 1.28 μm, 0.93 μm and 0.21 μm, respectively, but the diameter of anodic TiO_2 nanotubes was almost the same, at about 164 nm. When the temperature was low, the magnitude of electronic current and the ionic current was small, the mold effect was weak and nanotubes could not be formed. At the same time, this study shows that the dissolution reaction of the field-assisted solution theory has no electron gain or loss, and it has nothing to do with the current, which negates the field-assisted dissolution theory. A novel two-step anodization was used to verify the conclusion. It was found that nanotubes could be obtained when the anodizing current was decreasing or increasing. Also, ginseng-shaped nanotubes are formed at a particular voltage sequence. Based on the 'oxygen bubble model' and the ionic current and electronic current theories, the formation process of nanotubes of two-step anodization is explained clearly.

Received 6th September 2021
Accepted 23rd November 2021

DOI: 10.1039/d1ra06694c

rsc.li/rsc-advances

1. Introduction

There are normally three types of TiO_2 synthesis methods: the template method, hydrothermal synthesis method and electrochemical anodization.

(1) Template synthesis method: the preparation of nanotubes by assembling nanostructured elements into template holes, but this kind of prepared TiO_2 nanotube films does not show superior performance in electronic screening, photoelectric conversion and other aspects, indicating that the best performance of TiO_2 nanotubes is closely related to the preparation method.[1]

(2) Hydrothermal synthesis method: nano-TiO_2 powder is reacted with a concentration of about 10 mol L^{-1} of an alkali solution (NaOH solution) in a high-pressure reaction vessel, and the reaction temperature is controlled at 110–120 °C. After the reaction, the product is aged, washed, and heat-treated to obtain the final product TiO_2 nanotubes. However, this kind of TiO_2 nanotube film is disordered, difficult to control the number of tube layers, and difficult to establish the structure–activity relationship.

(3) Electrochemical anodization and porous anodic oxides have received extensive attention because such nanomaterials have broad application prospects in many fields.[2–6] However, the formation mechanism of anodic TiO_2 nanotubes is still in debate.[7–13] The field-assisted dissolution theory[14–17] is the most classical, believing that the field-assisted dissolution of the oxide gives rise to the formation of anodic TiO_2 nanotubes. But many recent findings cannot be explained *via* the field-assisted dissolution theory.[18–23] Zhou *et al.* reported that the growth rate of nanotubes in electrolytes with 2 wt% H_2O was significantly faster than that in electrolytes with 10 wt% H_2O.[24] Zhang *et al.* suggested that the growth rate of nanotubes had nothing to do with the concentration of NH_4F.[25]

In addition to studying the effects of water and fluoride ions, researchers have also explored many other factors that influence the growth of anodic TiO_2 nanotubes, such as voltage and temperature.[26–28] Mohan *et al.* reported that higher temperature caused a rise in the dissolution rate of oxides.[29] Schmuki *et al.* suggested that the growth-transition of a nanotubular TiO_2 into a hexagonally shaped TiO_2 nanocolumnar morphology can be obtained under a control film temperature at a sufficiently high applied potential anodized in a fluoride-containing organic electrolyte.[30]

[a]School of Chemistry and Chemical Engineering, Nanjing University of Science and Technology, Nanjing 210094, China. E-mail: liulin@jou.edu.cn; soong_ye@sohu.com

[b]School of Environmental and Chemical Engineering, Jiangsu Ocean University, Lianyungang 222005, China

† Authors Tianle Gong and Jieda Chen contributed equally to this work.

© 2022 The Author(s). Published by the Royal Society of Chemistry

Open Access Article. Published on 22 December 2021. Downloaded on 11/8/2025 3:00:16 AM.
This article is licensed under a Creative Commons Attribution-NonCommercial 3.0 Unported Licence.

However, most researchers chose to study the synthesis at ambient temperature or above and they cannot explain many experimental results with the field-assisted dissolution theory.[29–31] Most of the researchers believe that at a relatively low temperature, only the compact oxide layer can form, and the dissolution of the electrolyte will cause shallow pits on the surface of the compact oxide layer. However, in this study, the growth of anodic TiO_2 nanotubes was studied at low temperature for the first time and gourd-shaped nanotube embryos were found. These gourd-shaped nanotube embryos are strong evidence to prove the existence of oxygen bubbles. How can the weak dissolution of the electrolyte at low temperature lead to the gourd-shaped nanotube embryos? The interesting morphology of nanotubes cannot be explained by the field-assisted dissolution theory. Few papers before have explained the essence of the current–time curve as it changes with temperature. The connection between the current–time curve and the morphology of the nanotubes has not yet been explored. That is because the field-assisted dissolution reaction itself has nothing to do with the current. A new explanation for the decreasing current under low temperature is given based on the 'oxygen bubble model'[32–38] and the ionic current and electronic current theories.[39–45] We propose that the electronic current, rather than the field-assisted dissolution, plays an important role in the growth of nanotubes. During the anodization, the electronic current leads to the formation of oxygen bubbles. The oxygen bubbles serve as a mold, around which oxides grow and form anodic TiO_2 nanotubes. The formation of nanotubes is not the result of the field-assisted dissolution of the electrolyte.[46–48]

This result was confirmed from an interesting two-layer nanotube array obtained using a novel two-step anodization process. Herein, two voltage sequences of anodization are designed to form nanotubes. It is found that nanotubes can form whenever the current keeps decreasing or increasing, which questions the field-assisted dissolution equilibrium. Also, the 'oxygen bubble model' is used to explain the boundary between the nanotubes of two anodization. In addition, ginseng-shaped nanotubes are found. Based on the ionic current and electronic current theories, a clear explanation is given to explain the interesting morphology of nanotubes.

2. Experimental details

The experiment was divided into two parts. The details are presented as follows. The experiments were repeated twice for each sample under each condition to ensure that the current curve was consistent.

2.1 Part 1: temperature control in Ti anodization

Titanium foils with a purity of 99.5% and thickness of 100 μm were selected. The anodization area was maintained at 1.0 cm × 2.0 cm × 2 sides. Before the anodization, they were polished for 20 seconds using a mixed solution of HF, HNO_3 and deionized water (1 : 1 : 2 by volume). The surface of titanium foils was free of scratches. The samples were then rinsed thoroughly with deionized water and put in the air for drying. The titanium foil functioned as the anode and a platinum plate served as the cathode.

These titanium foils were anodized separately in ethylene glycol electrolyte containing 0.5 wt% NH_4F and 2 wt% H_2O under different temperatures (15, 0 and −10 °C) at a constant voltage (60 V) for 600 seconds.

2.2 Part 2: two-step anodization of Ti

The cutting and polishing process is as same as that described in part 1. During anodization, the titanium foil was used as the anode and a graphite plate served as the cathode. The anodization area was also maintained at 1.0 cm × 2.0 cm × 2 sides.

Two-layer nanotubes were obtained by a novel two-step anodization. There were two sequences of anodization.

Sequence 1: the first anodization was conducted in ethylene glycol electrolyte containing 0.5 wt% NH_4F and 2 wt% H_2O at a constant voltage (60 V) for 600 seconds. The second anodization was conducted in the same electrolyte at a constant voltage (40 V) for 600 seconds.

Sequence 2: the first anodization was conducted in ethylene glycol electrolyte containing 0.5 wt% NH_4F and 2 wt% H_2O at a constant voltage (40 V) for 600 seconds. The second anodization was conducted in the same electrolyte at a constant voltage (60 V) for 600 seconds.

The anodizing temperature was maintained using a constant-temperature bath. The anodizing current was recorded throughout the experiment. The distance between the electrodes was kept constant at 2 cm. After anodization, all the samples were soaked in plenty of deionized water for an hour. Then, they were rinsed using deionized water and dried in air to remove the solute remaining on the surface of the oxide film. Finally, to observe the cross-section of the anodic films on the Ti, all samples were bent several times to artificially manufacture cracks so as to directly observe the cross-section of the nanotube. All the samples were characterized using a FESEM instrument (Zeiss Supra 55).

3. Results and discussion

3.1 Temperature control anodization of Ti

Fig. 1 shows FESEM images of the anodic oxide film showing the length and diameter of nanotubes anodized under a constant voltage of 60 V for 600 s and the corresponding current–time curves. When the anodizing temperature was 15 °C and 0 °C, lengths of anodic TiO_2 nanotubes were 1.28 μm and 0.93 μm, respectively, as shown in Fig. 1a and b. When the temperature dropped to −10 °C, as shown in Fig. 1c, only the anodic TiO_2 nanotube embryos were formed and the length of the anodic TiO_2 nanotube embryos was 0.21 μm. The diameter of the nanotubes or nanotube embryos under different temperatures was almost 164 nm. According to the field-assisted dissolution theory, the formation of anodic TiO_2 nanotubes is the result of the field-assisted dissolution of the electrolyte.[49] However, under a relatively low temperature, field-assisted dissolution should also exist. Only the nanotube

 © 2022 The Author(s). Published by the Royal Society of Chemistry

Open Access Article. Published on 22 December 2021. Downloaded on 11/8/2025 3:00:16 AM.
This article is licensed under a Creative Commons Attribution-NonCommercial 3.0 Unported Licence.

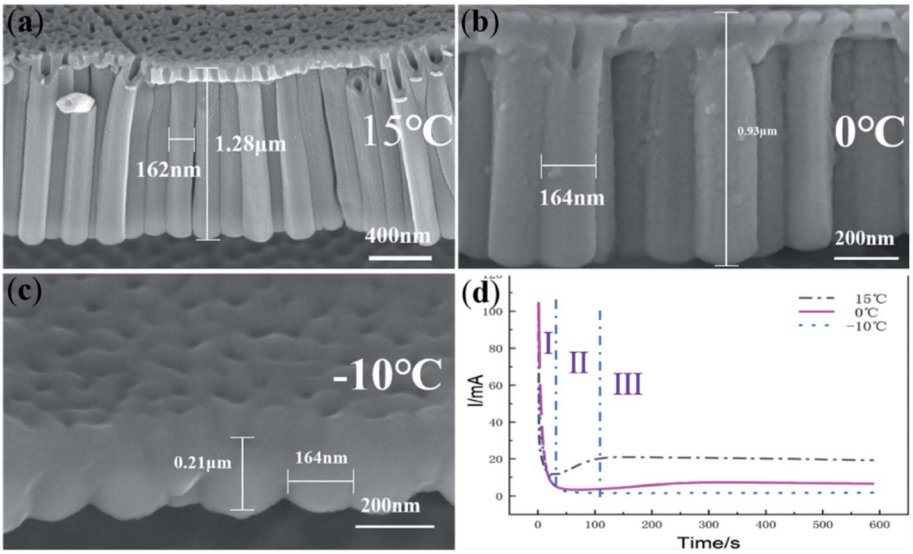

Fig. 1 FESEM images of TiO_2 nanotubes anodized at (a) 15 °C; (b) 0 °C; (c) −10 °C at a constant voltage 60 V and (d) the corresponding current–time curve.

embryos with a short length are formed, which the field-assisted dissolution theory cannot explain. Also, it is hard to give a clear explanation using the field-assisted dissolution theory to explain the three stages during the anodization of anodic TiO_2 nanotubes clearly. According to the field-assisted dissolution theory, porous anodic oxides form at the metal/oxide interface and are dissolved at the oxide/electrolyte interface ($TiO_2 + 6F^- + 4H^+ \rightarrow [TiF_6]^{2-} + 2H_2O$).[49–51] The rate of dissolution and growth is equal so that the current in the third stage (III) is kept the same. However, how the field-assisted dissolution can keep the equilibrium between the oxide growth and dissolution at different temperatures is not given a convincing explanation by the field-assisted dissolution theory. Zhang *et al.* suggested that the growth rate of nanotubes is much higher than the dissolution rate of nanotubes.[52] Besides, the field-assisted dissolution reaction has been denied by the flow model of the porous anodic film and it has been verified that equilibrium between oxide growth and dissolution is impossible.[53–55]

In the temperature control experiment, the fluoride ion concentration of the electrolyte did not change. According to the field-assisted dissolution theory, the dissolution reaction ($TiO_2 + 6F^- + 4H^+ \rightarrow [TiF_6]^{2-} + 2H_2O$) forms anodic TiO_2 nanotubes. However, there is no electron gain or loss in this reaction. This reaction is just a chemical dissolution reaction and does not contribute to the current. The difference in the current–time curve in Fig. 1d is not related to the dissolution reaction. That is to say, the formation of nanotubes is not the result of the field-assisted dissolution theory.

Fig. 2 is a diagram of the 'oxygen bubble model' growth. According to the 'oxygen bubble model'[32–38] and ionic current and electronic current theories.[39–45] Two reactions happened at the anode.

$$Ti - 4e^- + 2H_2O \rightarrow TiO_2 + 4H^+ \quad (1)$$

$$2H_2O - 4e^- \rightarrow O_2 + 4H^+ \quad (2)$$

A reaction was performed on the cathode.

$$4H_2O + 4e^- \rightarrow 2H_2 + 4OH^- \quad (3)$$

The total reaction equation:

$$Ti + 2H_2O \rightarrow TiO_2 + 2H_2 \quad (4)$$

$$2H_2O \rightarrow O_2 + 2H_2 \quad (5)$$

The ionic current controls the growth of oxide and the electronic current control the formation of oxygen bubbles. The compact oxide layer is the result of oxides caused by ionic current and the formation of anodic TiO_2 nanotubes is the result of oxygen bubbles caused by the electronic current, which may be expressed simply as:[34,35,39]

$$J_{total} = J_e + J_{ion} \quad (6)$$

$$J_{ion} = A\exp(\beta E) = A\exp(\beta U/d) \quad (7)$$

$$J_e = J_0\exp(\alpha d) \quad (8)$$

where J_{ion} is the ionic current, J_e is the electronic current, J_0 is the primary electronic current.[39] α, β and A are specific proportionality factors. E is the electric field strength. U is the voltage size and d is the thickness of the barrier oxide layer. The ionic current and electronic current are in direct and inversely proportional exponential relation with the thickness d of the barrier oxide layer, respectively. Take the current–time curve at 15 °C in Fig. 1d as an example. In stage (I), a compact oxide layer is formed rapidly (Fig. 2a). The compact oxide layer, which is near the interface of electrolyte will become an anion-

Open Access Article. Published on 22 December 2021. Downloaded on 11/8/2025 3:00:16 AM.
This article is licensed under a Creative Commons Attribution-NonCommercial 3.0 Unported Licence.

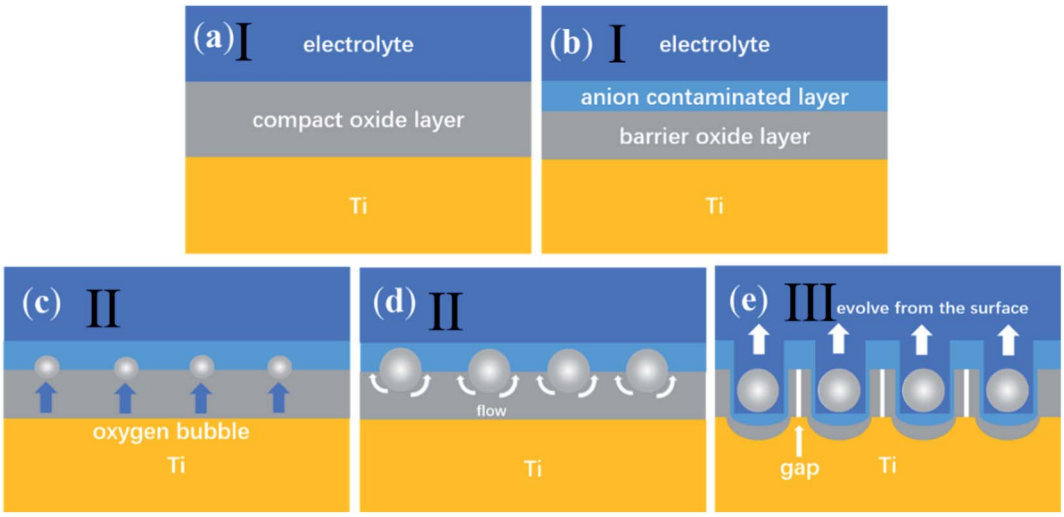

Fig. 2 Diagram of the 'oxygen bubble model' growth.

contaminated layer and the one, which is near the Ti will become a barrier oxide layer (Fig. 2b).[24,36] In the stage (II), when the ionic current declines to the minimum value, the barrier oxide layer reaches the critical thickness so as to generate J_e, which forms oxygen bubbles between the interface of the barrier oxide layer and the anion-contaminated layer (Fig. 2c).[19,20,56] The electronic current increases so oxygen bubbles continue to expand. However, under the pressure of the electrolyte and the anion-contaminated layer, oxygen bubbles cannot evolve at once. Thus, oxygen bubbles serve as a mold and the viscous flow of oxide can only grow around oxygen bubbles (Fig. 2d), which leads to the growth of nanotube embryos.[22] In stage (III), oxygen bubbles evolve from the surface of the nanotubes and the electrolyte reaches the bottom of the nanotubes.[9,20,56] Thus, the thickness of the barrier oxide layer remains the same as well as the ionic current. The ionic current and the electronic current run side by side. The ionic current produces oxide and the electronic current produces oxygen bubbles, growing into highly structured nanotubes.

According to the 'oxygen bubble model'[32–38] and the ionic current and electronic current theories,[39–45] when the temperature is high, the magnitude of electronic current and ionic current is large, so the mold effect is obvious, regular nanotubes can be formed, as shown in Fig. 1a. When the temperature is low, the magnitude of electronic current and ionic current is small, the mold effect is not obvious. The nanotube embryos grow slowly, so it is difficult to form nanotubes, as shown in Fig. 1c.

The field-assisted dissolution theory also cannot explain the diameter of nanotubes. According to the field-assisted dissolution theory, under low temperature, the dissolution of the electrolyte is weak so that the diameter of nanotubes will be small. However, the diameter of nanotubes under different temperatures is almost the same, about 164 nm, which is hard to explain using the field-assisted dissolution theory.

According to the ionic current and electronic current theories, the diameter of nanotubes is determined by the thickness of the anion-contaminated layer,[34,35,39] which is influenced by the magnitude of voltage. The temperature control anodization was conducted under a constant voltage of 60 V. Thus, the diameter of nanotubes under different temperatures is almost the same.

Fig. 3 shows the surface morphologies of nanotubes anodized at different temperatures. Fig. 3a shows that there are a lot of deep pores and shallow pits on the surface and the number of shallow pits is dramatically larger than the number of deep pores. The deep pores represent nanotubes. Shallow pits and deep pores on the surface appear to be randomly distributed. However, the nanotubes in Fig. 1 grow very regularly. According to the 'oxygen bubble model' and the ionic current and electronic current theories, the growth rate of nanotubes in the same sample is inhomogeneous and some oxygen bubbles have not evolved from the inside of nanotubes entirely.[9] Thus, some nanotubes hide under the compact oxide layer and cannot be seen from the surface, which gives a convincing explanation for the disordered distribution of deep pores. It indicates that the formation of shallow pits is a result of the dissolution of the electrolyte, which makes almost no contribution to the growth of nanotubes. Even, the deep pores almost disappear when the anodizing temperature drops to −10 °C in Fig. 3c. That is consistent with the gourd-shaped nanotube embryos in Fig. 1c. According to the field-assisted dissolution theory, at a low temperature, only the compact oxide layer and some shallow pits on the surface can be formed as a result of the weak dissolution of the electrolyte. However, it is hard for the field-assisted dissolution theory to explain the gourd-shaped nanotube embryos formed at −10 °C. How can the weak dissolution of the electrolyte at a low temperature form these gourd-shaped nanotube embryos? These gourd-shaped nanotube embryos are strong evidence to prove the correctness of the 'oxygen bubble model' and the ionic current and the electronic current theories. When the electrical current is small, many nanotube embryos have not opened yet, so the deep pores in the nanotube are not visible. However, shallow pits are always on the surface.

 © 2022 The Author(s). Published by the Royal Society of Chemistry

Open Access Article. Published on 22 December 2021. Downloaded on 11/8/2025 3:00:16 AM.
This article is licensed under a Creative Commons Attribution-NonCommercial 3.0 Unported Licence.

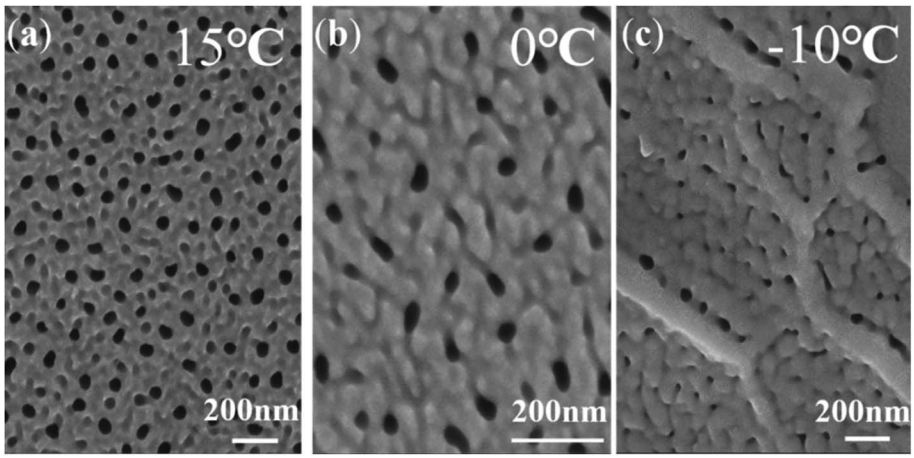

Fig. 3 FESEM images showing the surface morphologies of nanotubes anodized at a constant voltage (60 V) for 600 s at different temperatures: (a) 15 °C, (b) 0 °C, (c) −10 °C.

This result also verifies that the field-assisted dissolution always exists in the anodization and the effect of the field-assisted dissolution is very weak.[46]

3.2 Two-step anodization of Ti

Fig. 4 shows the current–time curve of the two-step anodization of Ti under 15 °C. The first anodization of sequence 1 is under 40 V (Fig. 4a), and the second anodization is under 60 V (Fig. 4b). The first anodization of sequence 2 is under 60 V (Fig. 4c), and the second anodization is under 40 V (Fig. 4d). It can be found that for both sequence 1 and sequence 2, the first anodization shows a normal three-stage curve, while for the second anodization in sequence 1, the current begins to decline slowly when it rapidly drops to 33 mA (Fig. 4b). In the second anodization of sequence 2, the current rapidly drops to 0.5 mA and then slowly rises (Fig. 4d). Nanotubes were found in both sequence 1 and sequence 2 (Fig. 5). According to the field-assisted dissolution theory, nanotubes result from the

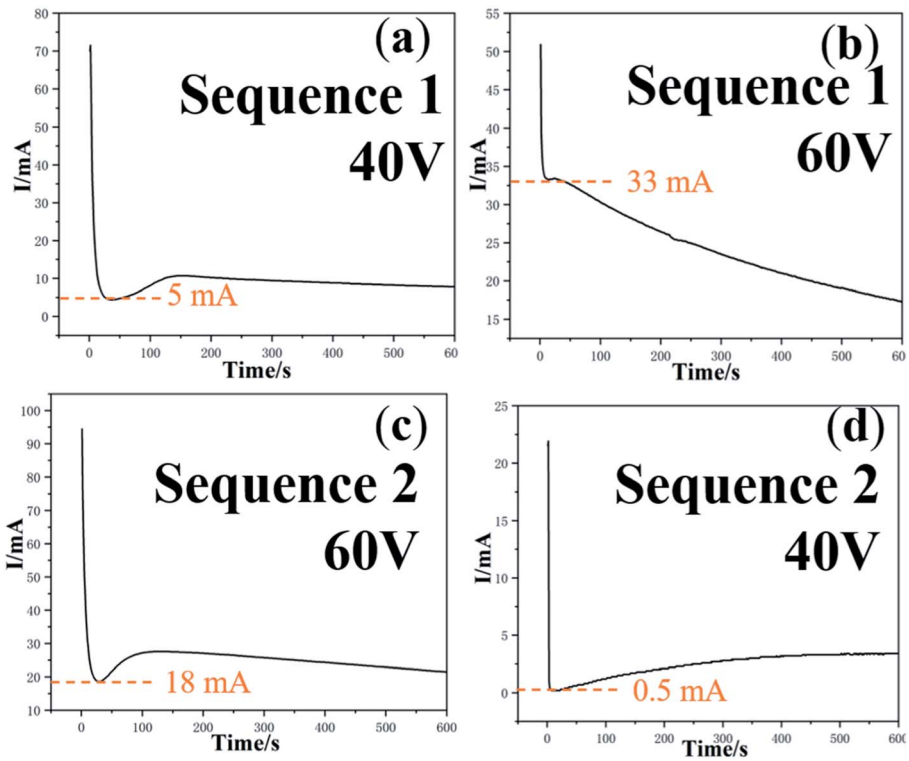

Fig. 4 The current–time curves corresponding to the two voltage sequences of two-step anodization: sequence 1 (a) and (b) 40 V + 60 V; sequence 2 (c) and (d) 60 V + 40 V.

Open Access Article. Published on 22 December 2021. Downloaded on 11/8/2025 3:00:16 AM.
This article is licensed under a Creative Commons Attribution-NonCommercial 3.0 Unported Licence.

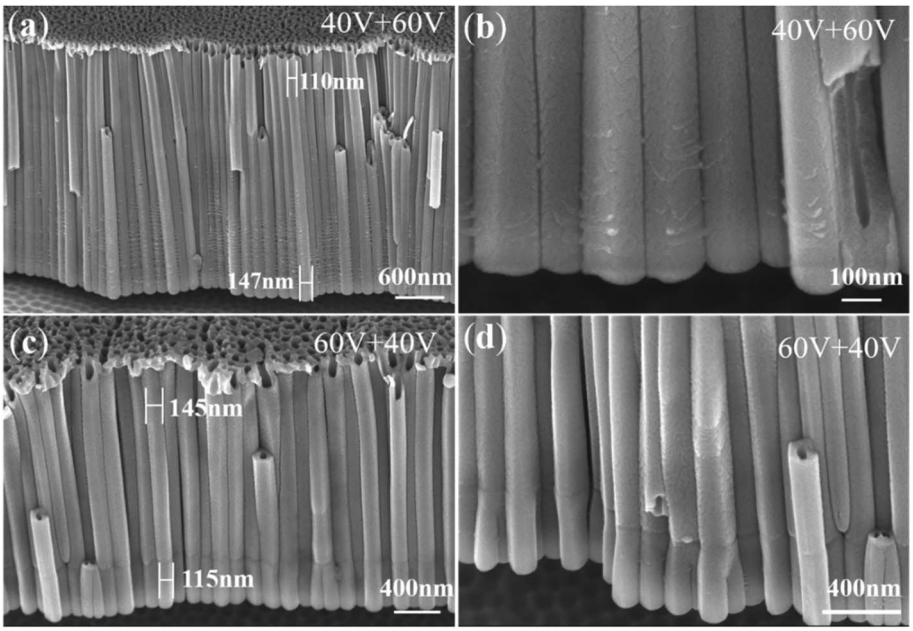

Fig. 5 FESEM images showing the two-layer nanotube arrays obtained by two-step anodization under different voltage sequences: sequence 1. (a) and (b) the first is 40 V, the second is 60 V; sequence 2. (c) and (d) the first is 60 V, the second is 40 V.

equilibrium between the dissolution of the electrolyte and the formation of the oxide, which leads to a stable current in the stage (III). However, in this two-step anodization experiment, the current of the second anodization in sequence 1 is increasing and in sequence 2 is decreasing. Both, sequence 1 and sequence 2 form nanotubes. This interesting result counters the dissolution equilibrium of the field-assisted dissolution theory. According to the equation of the ionic current and electronic current theories above,[34,35,39]

$$J_{\text{ion}} = A\exp(\beta E) = A\exp(\beta U/d) \tag{9}$$

$$J_{\text{e}} = J_0\exp(\alpha d) \tag{10}$$

When the current in the anodization declines, the ionic current dominates and more oxide is produced. When the current increases, the electronic current dominants and oxygen bubbles are produced more. That is to say, when the current drops rapidly, the oxygen bubble cannot serve the mold effect, and the compact oxide layer will be formed. When the current rises rapidly, the breakdown will occur, and the oxygen bubble will evolve directly. Only when the ionic current and electronic current are in a relatively balanced state, the oxide grows together with the oxygen bubble, and highly structured nanotubes can be formed. Thus, nanotubes can be formed in both, sequence 1 and sequence 2.

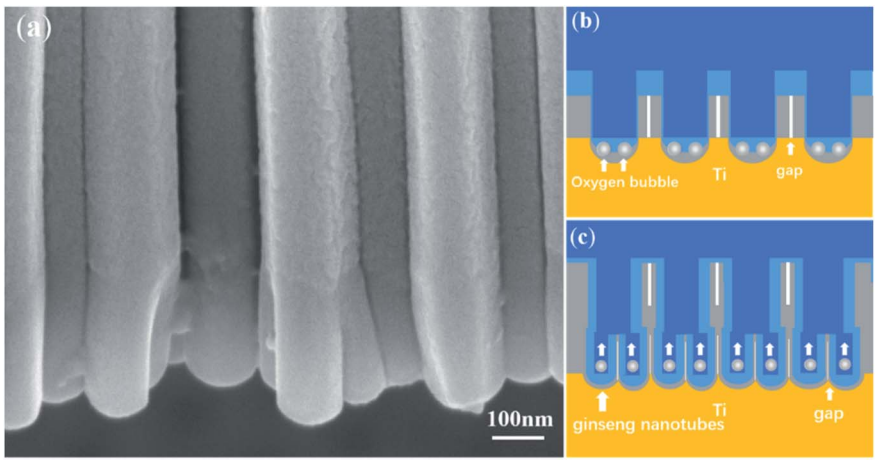

Fig. 6 FESEM images of (a) ginseng nanotubes were obtained in sequence 2 and (b) and (c) the schematic diagram of the ginseng nanotube growth.

 © 2022 The Author(s). Published by the Royal Society of Chemistry

Open Access Article. Published on 22 December 2021. Downloaded on 11/8/2025 3:00:16 AM.
This article is licensed under a Creative Commons Attribution-NonCommercial 3.0 Unported Licence.

Fig. 5 shows FESEM images of two-layer nanotube arrays obtained by two-step anodization for 600 s under two different voltage sequences. Fig. 5a and b show sequence 1 (40 V + 60 V). Fig. 5c and d show sequence 2 (60 V + 40 V). It can be seen that the diameter of the upper nanotubes in sequence 1 is smaller (about 110) nm and the diameter of the lower nanotubes in sequence 2 is larger (about 147 nm). The boundary between the two anodization cannot be seen in sequence 1, while it can be seen very clearly in sequence 2. This finding is hard for the field-assisted dissolution theory to explain.

According to the ionic current and electronic current theories,[39–45] for sequence 1, the voltage of the second anodization is higher, so the diameter of the lower nanotubes is larger than the diameter of the upper nanotubes. The total anodizing current keeps decreasing, indicating that the ionic current plays a leading role to form a thicker barrier oxide (Fig. 4b). As a result, more oxides are produced and the viscous flow of oxides grows from the bottom to the top and covers the boundary, forming a nanotube that is thick at the bottom and thin at the top, as shown in Fig. 5a.[57]

For sequence 2, due to the low voltage of the second anodization, the diameter of the lower nanotubes is smaller than the diameter of the upper nanotubes, while the total anodizing current keeps rising slowly (Fig. 4d), indicating that the electronic current dominates and less oxides are produced. Therefore, there are not enough oxides to grow upward to cover the boundary. Thus, the boundary between the two-layer nanotube arrays formed in the two anodization ins 2 can be clearly seen in Fig. 5c.

Fig. 6a shows a locally enlarged view of nanotubes from sequence 2, where the forked nanotubes, namely, ginseng nanotubes, can be clearly seen. According to the field-assisted dissolution theory, nanotubes are generated by the dissolution of the electrolyte.[49] According to the field-assisted dissolution theory, the number of nanotubes in both layers should be equal. It is impossible to produce forked nanotubes as shown in Fig. 6a. There are obvious gaps between the ginseng nanotubes as shown in Fig. 6a. How can the dissolution of the electrolyte cause obvious gaps between each ginseng nanotube?

According to the 'oxygen bubble model' and the ionic current and electronic current theories,[39–45] when the second anodization is conducted in sequence 2, the voltage (40 V) of the second anodization is lower than that of the first anodization (60 V). In this way, under a lower electric field, more electronic current can only be generated (Fig. 4d), leading to more oxygen evolution (Fig. 6b). A voltage of 40 V leads to a thinner barrier oxide layer. Accordingly, a larger number of nanotubes with smaller diameters were formed in the second layer, that is, ginseng-shaped nanotubes as shown in Fig. 6b and c were formed.

4. Conclusions

There are two groups of experiments in this paper, one is the single factor experiment, temperature control anodization, the other is two-step anodization. In the temperature control anodization, the length of anodic TiO_2 nanotubes at 15 °C, 0 °C, −10 °C is 1.28 μm, 0.93 μm and 0.21 μm, but the diameter of anodic TiO_2 nanotubes is almost the same, at about 164 nm. We also proposed the 'oxygen bubble model' and the ionic current and electronic current theories to explain in detail the morphology difference of nanotubes at different temperatures. When the temperature is high, the magnitude of electronic current and ionic current is large, so the mold effect is obvious, regular nanotubes can form. While at a low temperature, nanotubes are hard to form as a result of the low electronic current and ionic current.

In the two-step anodization, we designed the anodization of two voltage sequences, and nanotubes are obtained whenever the current continues to fall or the current continues to rise, denying the traditional theory that the dissolution equilibrium produces nanotubes. A new type of ginseng nanotube is found. According to the ionic current and electronic current theories, when the electronic current is low, the diameter of nanotubes will become smaller. Due to the bottom-up growth mode, the oxide grows around the small oxygen bubble at the bottom of the first anodization to form ginseng nanotubes. These interesting results presented in this work are of help to get a better comprehension of the growth mechanism of porous anodic oxides.

Author contributions

Tianle Gong: methodology, writing – original draft. Jieda Chen: methodology, writing – review & editing, formal analysis. Pengjin Fang: writing – review & editing, investigation. Lin Liu: conceptualization, project administration. Chengyuan Li: formal analysis, validation. Aijun Han: supervision. Ye Song: supervision.

Conflicts of interest

The authors declare that they have no known competing financial interests or personal relationships that could have appeared to influence the work reported in this paper.

Acknowledgements

This work was financially supported by the National Natural Science Foundation of China (Grant No. 51777097, 51577093) and the National Undergraduate Training Program for Innovation and Entrepreneurship (202110288048).

References

1 Q. Y. Wang, H. L. Li, X. L. Yu, Y. Jia, Y. Chang and S. M. Gao, *Electrochim. Acta*, 2020, **330**, 135167.
2 A. Ruiz-Clavijo, O. Caballero-Calero and M. Martín-González, *Nanoscale*, 2021, **13**, 2227–2265.
3 S. Y. Cao, D. L. Yu, Y. Lin, C. Zhang, L. F. Lu, M. Yin, X. Zhu, X. Y. Chen and D. Li, *ACS Appl. Mater. Interfaces*, 2020, **12**, 26184–26192.
4 L. Shen, Y. Li, W. Zhong, J. C. Wu, J. H. Cheng, L. Jin, X. Hu and Z. Y. Ling, *Electrochem. Commun.*, 2021, **126**, 107014.

Open Access Article. Published on 22 December 2021. Downloaded on 11/8/2025 3:00:16 AM.
This article is licensed under a Creative Commons Attribution-NonCommercial 3.0 Unported Licence.

5 Z. Y. Yuan, S. W. Zhang, F. L. Meng, H. Zhang and K. Y. Zuo, *IEEE Sens. J.*, 2020, **20**, 4275–4282.
6 C. P. Yu, Z. L. Zheng, W. C. Zhang, B. Hu, Y. J. Chen, J. H. Chen, K. F. Ma, J. H. Ye and J. W. Zhu, *ACS Sustainable Chem. Eng.*, 2020, **8**, 3969–3975.
7 K. R. Hebert, S. Albu, I. Paramasivam and P. Schmuki, *Nat. Mater.*, 2012, **11**, 162–166.
8 H. Tsuchiya and P. Schmuki, *Nanoscale*, 2020, **12**, 8119–8132.
9 T. L. Gong, C. Y. Li, X. Li, H. Y. Yue, X. F. Zhu, Z. Y. Zhao, R. Q. Lv and J. W. Zhu, *Nanoscale Adv.*, 2021, **3**, 4659–4668.
10 P. Z. Li, J. Wang, L. Liu, J. J. Ma, Y. L. Ni, H. Wang and Y. Song, *Electrochem. Commun.*, 2021, **132**, 107146.
11 K. Y. Wang, G. H. Liu, N. Hoivik, E. Johannessen and H. Jakobsen, *Chem. Soc. Rev.*, 2014, **43**, 1476–1500.
12 D. Regonini, C. R. Bowen, A. Jaroenworaluck and R. Stevens, *Mater. Sci. Eng., R*, 2013, **74**, 377–406.
13 S. Chen, Y. L. Ni, J. P. Zhang, Y. X. Dan, W. C. Zhang, Y. Song and X. F. Zhu, *Electrochem. Commun.*, 2021, **125**, 106991.
14 N. J. Suliali, C. M. Mbulanga, W. E. Goosen, R. Betz and J. R. Botha, *Electrochim. Acta*, 2020, **337**, 135791.
15 A. Gao, R. Hang, L. Bai, B. Tang and P. K. Chu, *Electrochim. Acta*, 2018, **271**, 699–718.
16 X. Li, C. Y. Li, T. L. Gong, J. H. Su, W. C. Zhang, Y. Song and X. F. Zhu, *Ceram. Int.*, 2021, **47**, 23332–23337.
17 D. J. LeClere, A. Velota, P. Skeldon, G. E. Thompson, S. Berger, J. Kunze, P. Schmuki, H. Habazaki and S. Nagata, *J. Electrochem. Soc.*, 2008, **155**, C487–C494.
18 Z. X. Su and W. Z. Zhou, *J. Mater. Chem.*, 2011, **21**, 8955–8970.
19 M. S. Yu, C. Li, Y. B. Yang, S. K. Xu, K. Zhang, H. M. Cui and X. F. Zhu, *Electrochem. Commun.*, 2018, **90**, 34–38.
20 Y. L. Ni, J. Zhang, T. L. Gong, M. Sun, Z. Y. Zhao, X. Li, H. W. Yu and X. F. Zhu, *Surf. Interfaces*, 2021, **26**, 101419.
21 J. Zhang, Y. T. Yu, P. J. Fang, L. Liu, H. Y. Yue, J. L. Ou and A. J. Han, *Electrochem. Commun.*, 2021, **129**, 107086.
22 Q. Y. Zhou, M. M. Tian, Z. R. Ying, Y. X. Dan, F. R. Tang, J. P. Zhang, J. W. Zhu and X. F. Zhu, *Electrochem. Commun.*, 2020, **111**, 106663.
23 Z. Y. Zhang, Q. Wang, H. Q. Xu, W. C. Zhang, Q. Y. Zhou, H. P. Zeng, J. L. Yang, J. W. Zhu and X. F. Zhu, *Electrochem. Commun.*, 2020, **114**, 106717.
24 Q. Y. Zhou, D. M. Niu, X. J. Feng, A. C. Wang, Z. R. Ying, J. P. Zhang, N. Lu, J. W. Zhu and X. F. Zhu, *Electrochem. Commun.*, 2020, **119**, 106815.
25 Z. Y. Zhang, Q. Q. Liu, M. F. He, F. R. Tang, Z. R. Ying, H. Q. Xu, Y. Song, J. W. Zhu and X. F. Zhu, *J. Electrochem. Soc.*, 2020, **167**, 113501.
26 J. Kapusta-Kołodziej, O. Tynkevych, A. Pawlik, M. Jarosz, J. Mech and G. D. Sulka, *Electrochim. Acta*, 2014, **144**, 127–135.
27 G. D. Sulka, J. Kapusta-Kolodziej, A. Brzózka and M. Jaskula, *Electrochim. Acta*, 2013, **104**, 526–535.
28 B. Lucas-Granados, R. Sanchez-Tovar, R. M. Fernandez-Domene and J. Garcia-Anton, *Int. J. Hydrogen Energy*, 2018, **43**, 7923–7937.
29 L. Mohan, C. Dennis, N. Padmapriya, C. Anandan and N. Rajendran, *Mater. Today Commun.*, 2020, **23**, 101103.
30 T. Ruff, R. Hahn and P. Schmuki, *Appl. Surf. Sci.*, 2011, **257**, 8177–8181.
31 N. S. Peighambardoust and F. Nasirpouri, *Surf. Coat. Technol.*, 2013, **235**, 727–734.
32 J. W. Cao, Z. Q. Gao, C. Wang, H. M. Muzammal, W. Q. Wang, Q. Gu, C. Dong, H. T. Ma and Y. P. Wang, *Surf. Coat. Technol.*, 2020, **388**, 125592.
33 X. F. Zhu, L. Liu, Y. Song, H. B. Jia, H. D. Yu, X. M. Xiao and X. L. Yang, *Monatsh. Chem.*, 2008, **139**, 999–1003.
34 X. F. Zhu, Y. Song, L. Liu, C. Y. Wang, J. Zheng, H. Jia and X. Wang, *Nanotechnology*, 2009, **20**, 475303.
35 X. F. Zhu, Y. Song, D. Yu, C. Zhang and W. Yao, *Electrochem. Commun.*, 2013, **29**, 71–74.
36 P. Y. Deng, X. D. Bai, X. W. Chen and Q. L. Feng, *J. Electrochem. Soc.*, 2004, **151**, B284–B289.
37 J. W. Cao, C. Wang, Z. Q. Gao, S. Y. Shang, Q. D. Gu, N. Gao, Y. P. Wang and H. T. Ma, *ECS J. Solid State Sci. Technol.*, 2020, **9**, 104010.
38 L. Li, Z. X. Zhang, L. L. Bo, Y. J. Cui, Y. M. Xu and Z. F. Zhang, *Surf. Coat. Technol.*, 2020, **404**, 126470.
39 J. M. Albella, I. Montero and J. M. Martinez-Duart, *Electrochim. Acta*, 1987, **32**, 255–258.
40 Y. Li, Z. Y. Ling, X. Hu, Y. Liu and Y. Chang, *RSC Adv.*, 2012, **2**, 5164–5171.
41 B. Chong, D. Yu, R. Jin, Y. Wang, D. Li, Y. Song, M. Gao and X. Zhu, *Nanotechnology*, 2015, **26**, 145603.
42 A. D. Pauric, S. A. Baig, A. Pantaleo, Y. Wang and P. Kruse, *J. Electrochem. Soc.*, 2013, **160**, C12–C18.
43 D. Li, L. Zhao, C. H. Jiang and J. G. Lu, *Nano Lett.*, 2010, **10**, 2766–2771.
44 S. W. Zhao, J. Xing, H. W. Fan, S. Y. Zhang, D. Li and X. F. Zhu, *J. Electrochem. Soc.*, 2017, **164**, E187–E193.
45 S. W. Zhao, T. Lu, H. M. Cui, D. L. Yu, S. Y. Zhang, J. S. Kong and X. F. Zhu, *J. Electrochem. Soc.*, 2017, **164**, E401–E407.
46 O. O. Capraz, P. Shrotriya, P. Skeldon, G. E. Thompson and K. R. Hebert, *Electrochim. Acta*, 2015, **167**, 404–411.
47 Y. Zhang, W. Cheng, F. Du, S. Y. Zhang, W. Ma, D. Li, Y. Song and X. F. Zhu, *Electrochim. Acta*, 2015, **180**, 147–154.
48 H. Lu, H. Fan, R. Jin, B. Chong, X. Shen, S. Yan and X. F. Zhu, *Electrochim. Acta*, 2016, **215**, 380–387.
49 R. Q. Hang, F. L. Zhao, X. H. Yao, B. Tang and P. K. Chu, *Appl. Surf. Sci.*, 2020, **517**, 146118.
50 F. Riboni, N. T. Nguyen, S. So and P. Schmuki, *Nanoscale Horiz.*, 2016, **1**, 445–466.
51 D. S. Guan and Y. Wang, *Nanoscale*, 2012, **4**, 2968–2977.
52 Y. Zhang, W. Cheng, F. Du, S. Y. Zhang, W. Ma, D. Li, Y. Song and X. F. Zhu, *Electrochim. Acta*, 2015, **180**, 147–154.
53 G. E. Thompson, *Thin Solid Films*, 1997, **297**, 192–201.
54 S. X. Liu, J. L. Tian and W. Zhang, *Nanotechnology*, 2021, **32**, 222001.
55 N. Lu, J. P. Zhang, Y. X. Dan, M. Sun, T. L. Gong, X. Li and X. F. Zhu, *Electrochem. Commun.*, 2021, **126**, 107022.
56 R. Jin, M. Y. Liao, T. Lin, S. Y. Zhang, X. P. Shen, Y. Song and X. Zhu, *Mater. Res. Express*, 2017, **4**, 065008.
57 J. J. Zhang, W. Q. Huang, K. Zhang, D. Z. Li, H. Q. Xu and X. F. Zhu, *Electrochem. Commun.*, 2019, **100**, 48–51.

 © 2022 The Author(s). Published by the Royal Society of Chemistry